Deliverable Report

Deliverable No: D6.1

Deliverable Title: Efficient calibration toolbox for complex reconfigurable interferometers

Grant Agreement number: 899544

Project acronym: PHOQUSING

Project title: PHOtonic Quantum SamplING machine

Project website address: www.phoqusing.eu

Name, title and organisation of the scientific representative of deliverable's lead beneficiary (task leader):
Prof. Fabio Sciarrino, Università di Roma "La Sapienza"
Email: fabio.sciarrino@uniroma1.it

Deliverable table

Deliverable no.	D6.1
Deliverable name	Efficient calibration toolbox for complex reconfigurable interferometers
WP no.	6
Lead beneficiary	UNIROMA1
Type	Report
Dissemination level	Public
Delivery date from Annex I	M18
Actual delivery date	28 February 2022

What was planned *(from Annex I:)*

D6.1: Efficient calibration toolbox for complex reconfigurable interferometers [18]
Calibration of complex reconfigurable circuits represents a progressively demanding task when the size of system increases, given the large number of integrated components. Different techniques for the characterization of large size integrated systems will be developed and tested, in order to provide an efficient toolbox to calibrate and program the operation of the reconfigurable interferometers.

What was done

Nowadays multi-mode optical interferometers are fundamental building blocks of modern optics. They represent the most viable platforms for successful implementation of several computation schemes that take advantage of optical processing. Examples range from optical neural networks, optical reservoir computing, optical simulation of complex physical systems, metrology schemes, to the emergent applications in quantum computation and information protocols.
The realization of such routines requires high levels of control and tunability of the parameters that individuate the optical operations. More precisely, successful implementations of optical-based algorithms with multi-port interferometers require two main preliminary calibration stages. The first one is a strong and accurate reconstruction algorithm that individuates the element of the transfer matrix of the optical circuit from a suitable set of measurements. The second stage regards the ability to control the device to perform a given operation on the field modes, for instance via reconfigurable interferometers. These two calibrations become a not trivial task when the size of the interferometer is large and in the presence of experimental imperfections. In the following we describe the strategies developed within this deliverable for what concerns (i) reconstruction of the unitary matrix implemented by multi-port interferometers and (ii) calibration and correct tuning of reconfigurable circuits by exploiting optimization and machine learning-based algorithms. Note that the two methods are strongly interconnected. For example, a good reconstruction algorithm produces an accurate model that links the observed data to the optical circuit parameters. This is essential to build a good training set for further calibrations based on machine learning methods. On the other hand, black box approaches such as optimization and learning algorithms provide solutions for the task of circuit characterization when the response of the device is unknown.

(i) Reconstruction algorithms for multi-mode linear optical networks

Problem statement

Any linear operation $\hat{U}$ acting on the annihilation (creation) operators of the electromagnetic field in the mode i, i.e. operations that preserve the number of photons, can be expressed as follows

$$a_i \rightarrow \hat{U}^{\dagger} a_i \hat{U} = \sum_j U_{ji}\, a_j \qquad (1)$$

where U_{ji} is the unitary matrix representation in the Fock space of the operator $\hat{U}$. The same relation holds for classical states of light, by replacing the operators a_i with the complex field amplitudes E_i in the right-hand side of Eq. (*1*). In other words, matrix U_{ji} expresses how the field amplitudes propagate through a multi-mode linear optical network.

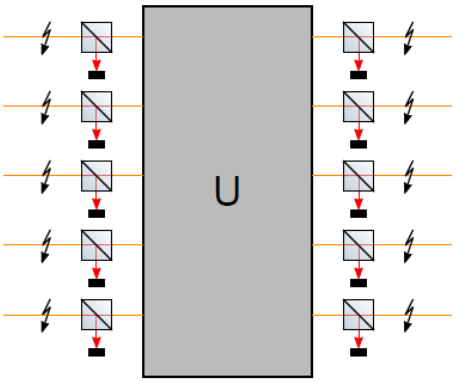

Figure 1. Model of a multi-port interferometer. We assume that a real interferometer can be seen as an ideal one implementing a unitary transformation U plus layers of input and the output losses (beam splitter in the figure) and phase instabilities (sparks) due to fiber connections.

Note that the optical modes i can be in principle any degree of freedom of light, such as polarization, path, time arrival, frequency, angular and transverse momentum.
Several algorithms have been proposed to reconstruct the matrix elements in the photonic community. One kind of approach aims at finding an analytic solution from single- and two-photon quantum measurements for individuating the elements of the matrix expressed in their polar representation, i.e. $U_{ij} = \tau_{ij}\, e^{i\,\phi_{ij}}$, without any assumption on the internal architecture of the interferometer [Laing2012]. Since this analytic method is not robust versus

the unavoidable noise of experimental data, alternative reconstruction algorithms look for the solution through numerical minimizations [Tillmann2016, Spagnolo2017]. In this last class of methods we can distinguish between black box approaches that exploit machine-learning and the procedures which include knowledge of the interferometer structure in the minimization.
In the following we report our results for what concerns a black-box approach for the reconstruction of the moduli $\tau_{ij}$and the phases ϕ_{ij}.

Losses and moduli estimation

We start our investigation from the estimation of the moduli τ_{ij}. We know that the τ_{ij}^2 is the probability to find a single-photon in the mode j given the initial mode i or, alternatively, the fraction of a classical field intensity in the mode j. This observation allows us to define the matrix $P_{ij} = \tau_{ij}^2$. However, in a single-photon or single laser beam intensity experiment it is not possible to measure the exact matrix due to the unavoidable mode-dependent photon losses that could exist in the preparation and collection stages (see Figure 1). Then the actual measured matrix M_{ij} can be modeled as follows

$$P = L_2 M L_1 \tag{2}$$

where $L_1$and $L_2$are diagonal matrices expressing the effect of the input and output losses respectively. The latter takes into account also eventual differences in the detection efficiencies among the modes.

The first approach we propose to solve Eq. (2) is the use of Sinkhorn's theorem which states that any doubly stochastic matrix can be decomposed into the product among two diagonal matrices and a matrix with real and non-negative entries [Sinkhorn1967], as in Eq. (2). There are several algorithms in literature based on this theorem to retrieve the matrices P, L_1, L_2 from the measurements in M [Idel2016]. The idea behind these algorithms is that in absence of losses the sum of the columns and rows of M should be one. Therefore, the algorithms try to normalize the rows and columns iteratively until the convergence is reached. They were formulated in contexts different from the photonic community. In this deliverable we applied these concepts to solve linear optical problems. We tested this method experimentally with a 3-mode integrated interferometer optical device and a continuous wave laser at the wavelength of 785 nm. The comparison between the measurements $M$and reconstructed matrix P that contains the true squared moduli of U is reported in Figure 2.

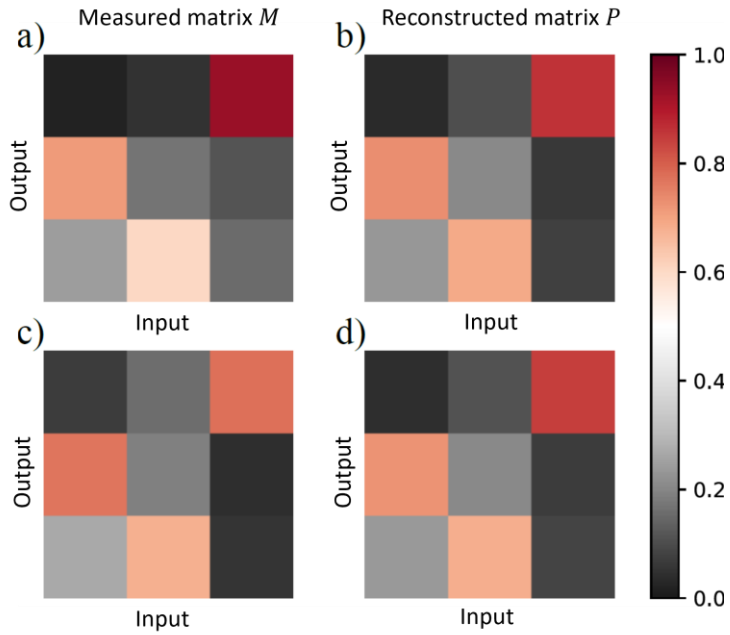

Figure 2. Application of the Sinkhorn theorem for the reconstruction of the squared moduli of the matrix of a 3-mode integrated chip. a) The input-output distribution of a continuous wave laser sent into the device. b) The matrix after the loss purification. c) Additional loss inserted in the third input. The algorithm retrieves again the correct distribution reported in d). The distributions in b) and d) have a fidelity of 99 % that proves the algorithm effectiveness in different lossy configurations.

The second approach exploits the reconfigurability of optical interferometers that change P but without affecting the loss matrices. Here we do not require to measure the field intensity distribution from each input port as in the previous method. In fact, this second method is effective even by

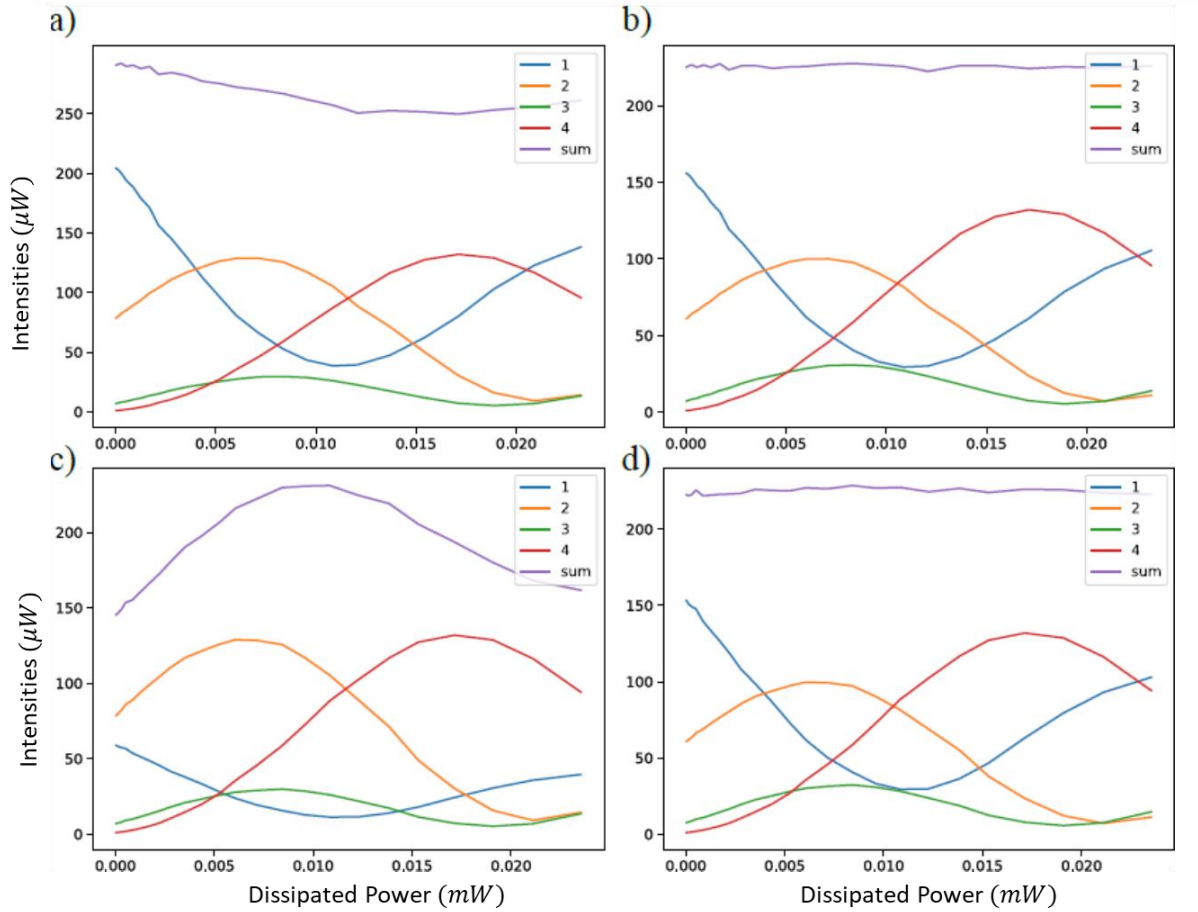

Figure 3. a) Recording of the field intensity at the outputs of a 4-mode reconfigurable integrated device for different settings of the dissipated electrical power in one heater. b) After the minimization of the variance, losses are identified and the curves corrected accordingly. c) Additional loss inserted in the output mode 1 that is corrected by the algorithm in the panel d). Note that the curves in b and d are the same. This confirms the effectiveness of the algorithm in different loss conditions.

injecting the radiation from one input and can thus be used to obtain information on a specific submatrix of the full evolution U. In this scenario we would be able to retrieve a column of P and the output losses L_2. This can be done by observing that the sum $S(\theta)$ of the measured column elements of $M = L_2 P$ is constant for any configuration θ of the optical circuit if the output losses are homogenous among the modes. Thus, in the most general scenario in which the losses are mode-dependent, we look for the diagonal matrix L_2 such that the variance of $S(\theta)$ is zero. For such a minimization an analytical solution can be found, but it can be solved also via a numerical approach which may present improved stability in the presence of experimental measurement errors.

We tested this second algorithm in a 4-mode reconfigurable optical circuit. The measurement was performed with a continuous wave laser at the wavelength of 785 nm injected in one of the input modes of the chip. The field intensities distribution in the 4 output ports was recorded via likewise power meters. In Figure 3a, we report the trends of the four measured intensities when we vary the dissipated power in one heater of the reconfigurable interferometer. In particular, the sum of the 4 signals is observed to be not constant, thus corresponding to a scenario of unbalanced losses. In Figure 3b, we report the same curves after applying the minimization of the variance of such a sum. In Figure

3c, we add an additional loss in the mode 1, while in Figure 3d we verify that the algorithm is able to recover again the correct distributions.

Reconstruction of the internal phases with classical light

In this section we show the possibility to reconstruct the internal phases of the matrix elements ϕ_{ij} with a classical light source. Previous methods use the visibility of Hong-Ou-Mandel (HOM) [Hong1987] effect for this task since it is not sensitive to input/output losses and phase instabilities [Laing2012]. However, the time needed to estimate HOM visibilities with an adequate accuracy is sometimes considerable due to the need of single-photon sources which limits the collection statistics. Here we show that an analogous quantity can be retrieved from the cross correlation between two coherent laser beams. The measurement scheme is presented in Figure 4a. The laser source is split and sent into the network in modes *(h,k)*. The additional phases φ_1 and φ_2 account for eventual phase instabilities in the optical paths between the sources and the interferometer. For example, these instabilities could be due to the input fiber connections that are sensitive to thermal and mechanical fluctuations. The cross correlation is defined as $C_{ij}^{hk} = 1 - \frac{<I_i\, I_j>}{<I_i><I_j>}$, where I_i and I_j are the field intensities in the corresponding output modes and $<\cdot>$ is the time average. We require that the external phase fluctuations $\varphi = \varphi_1 - \varphi_2$ have zero-time average. This his means to ask for $< e^{i\varphi} >= 0$ and $< e^{2i\varphi} >= 0$. In general, mechanical and thermal phase fluctuations of the fiber connections do not satisfy these conditions.

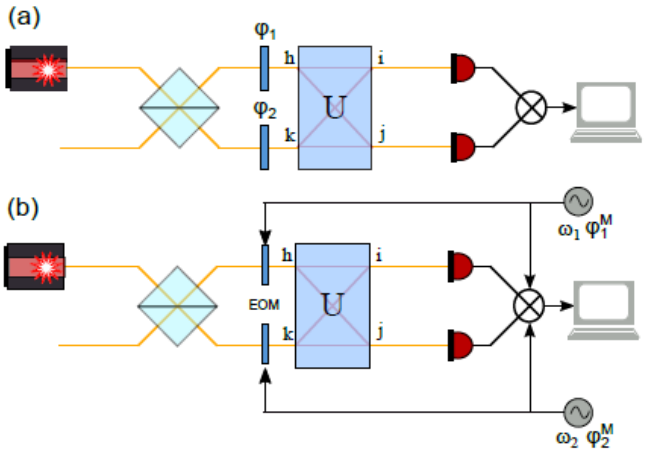

Figure 5. (a) Schematic of the apparatus for the reconstruction of the matrix phases with a classical light source. (b) Apparatus with phase and amplitude modulations via EOMs (electro-optic modulators) to remove the dependence from the input losses and phase fluctuation in the cross-correlation measurement.

This problem can be solved by adding a phase modulator in one of the two input paths. In the latter condition, the external phase contribution can be expressed as $< e^{i(\varphi_M+\varphi_T)} >$, where φ_M is the modulated phase and φ_T is the mechanical and the thermal noise. Since the two contributions are uncorrelated we can write $< e^{i(\varphi_M+\varphi_T)} >=< e^{i\varphi_M} >< e^{i\varphi_T} >$. This can be satisfied by controlling the phase modulation such that $< e^{i\varphi_M} >= 0$ and $< e^{2i\varphi_M} >= 0$, e.g., with a triangular modulation or through a white noise signal of appropriate amplitude. The residual dependence from the input losses can be removed by introducing an additional amplitude modulation with frequency ω (see Figure 4b). By averaging the intensities over time and ω, the final expression for the cross correlation is equivalent to the HOM visibility:

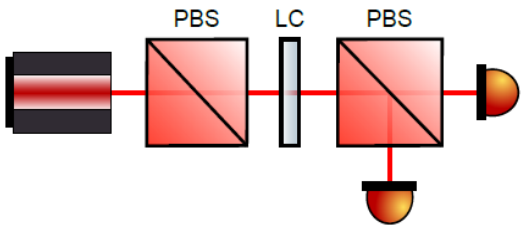

Figure 4. Apparatus for the proof-of-principle experiment with a Mach-Zehnder interferometer encoded in the polarization.

$$C_{ij}^{hk} = -\frac{2\tau_{ih}\tau_{ik}\tau_{jh}\tau_{jh}}{\tau_{ih}^2\tau_{jk}^2 + \tau_{jh}^2\tau_{ik}^2} cos(\phi_{ih} + \phi_{jk} - \phi_{ik} - \phi_{jh}) \qquad (3)$$

To test this method developed for the phase measurement, we performed two proof-of-principle experiments. The idea is to test the setup in Figure 5 by considering as U a second beam-splitter. The

resulting structure is equivalent to a Mach-Zehnder interferometer, that we implement in polarization via two polarizing beam-splitter (PBS) and an intermediate liquid-crystal (LC, with the slow axis at 45° with respect to the horizontal direction (see Figure 4). To satisfy the conditions $< e^{i\varphi_M} >= 0$ and $< e^{2i\varphi_M} >= 0$ we choose a discrete set of three angles $\{\varphi_0, \varphi_0 + \frac{2}{3}\pi, \varphi_0 + \frac{4}{3}\pi\}$ for the phase of the liquid crystal, instead of continuously varying the phase. In the preliminary stage we measure the input power and the efficiencies of the power-meters to take into account the input losses since we do not have an amplitude modulator operating at the right frequency at this moment in the laboratory. The result of the cross- correlation measurement was $C = 0.497 \pm 0.007$ that is compatible with the theoretical expected value of $C_{Theo} = 0.5$.

Such a method to retrieve HOM visibility-like quantities with classical light could speed up the time needed to collect enough data for the reconstruction of the phases. This could help in the collection of training sets for calibration based on neural networks or machine learning protocols, as we discuss below. For example, neural networks are a fundamental tool in absence of full knowledge on the transfer function between the control parameters of a large-scale reconfigurable interferometer, such as the dissipated electrical powers in the heaters, and the matrix elements.

(ii) Calibration of reconfigurable integrated optical circuit via neural networks

Reconfigurable 3-mode interferometer in single photon regime:
The problem of reconstructing the dynamic evolution of a circuit has been proven to be a difficult data analysis task, especially when the dimension of the system increases and the effect of noise becomes not negligible. The problem becomes particularly challenging when the circuit response function depends on the settings of different parameters and consequently on their relative cross-talks.

To investigate alternative calibration procedures which can be easily adapted to circuits with higher dimensions, we have studied the response function of an integrated multi-arm interferometer fabricated by femtosecond laser writing technique. The platform tested consists in a three-arm interferometer, representing the generalization of a 2-arm Mach-Zehnder interferometer and is represented in Figure 6a. Light injected into the device will undergo an evolution dependent on optical phase shifts. The device is capable to encode up to two independent optical phase shifts that can be manipulated through several thermo-optical phase shifters. The latter are integrated optical phase shifters which can be tuned by dissipating electrical currents by ohmic resistors. The correct calibration of the device response when different currents are applied is crucial in order to operate with the device.

Such a response depends on many parameters, both static and dynamical elements, since different resistors can be turned on. In general, the application of a pair of voltages (V_1, V_2) generates a different global phase shift, for a fixed input, along each optical path, resulting in a different action of the device. Therefore, the investigation of an efficient calibration method with different single photon input states is generally not trivial. The reconstruction of the response adopting the conventional method --- maximum likelihood estimation (MLE) based on fitting procedure --- in both single- and two-photon regimes has been demonstrated in [Polino2019]. This procedure requires a large amount of post-processing efforts, and a great amount of calibration data to obtain appropriate calibration results. Moreover, when the system complexity increases this approach is expected to be even more unpractical and not easily scalable to larger devices.

When interested only in the reconstruction of the output probability, related to the modulus of the coefficients of the circuit transformation matrix, a calibration procedure based on a neural network (NN) algorithm has proven to overcome the aforementioned issues [Cimini2021]. The strength of using a machine learning approach is that it does not require an analytic model of the device functioning, but it directly reconstructs from the observed data the map linking the voltages applied on the different resistors of the device and the single-photon output probabilities.

The device functioning can be studied by sending single photons in one of the three inputs and collecting the photon counts at the three outputs of the device. In this way, single-photon probabilities P_{ij} for each output j ($j = 1, 2, 3$) are measured by changing the input arm i of the single-photon state and tuning the power dissipated on the internal resistors. We tune the voltages applied to each resistor independently, while keeping the others off, studying the change in the outputs probabilities distributions. The set of collected data at the three outputs, for different values of tensions applied and for different inputs, is used to train the NN. More specifically, we measured the results obtained after the application of n different tensions values to each of the two resistors in the device. This gives a tension grid with $n \times n$ different tension pairs associated with the relative measured probabilities. Such data are successively used for the training.

We employ a feed-forward neural network, which is particularly suited for this purpose. After it has been trained, the NN is able to reconstruct the complex nonlinear map between a given input — the feature vector $\boldsymbol{x}$ — and the associated output vector $\boldsymbol{y}$. In our scenario $\mathbf{x}$ represents the measured output probabilities, while the vector $\boldsymbol{y}$ corresponds to the applied voltages. The structure of the implemented NN is shown in Figure 6b. It consists of a series of layers of nodes activated in cascade through non-linear activation functions.

In order to select the most suitable architecture for the NN we performed an initial study on a model emulating the functioning of a three-mode interferometer. Such preliminary study allowed us to identify the network architecture (number of nodes, layers, activation functions, initialization parameters) achieving higher performances and the amount of training data required to accomplish the calibration task. What we have found is that to achieve a good estimate in the full range of accessible tensions, it was necessary to incorporate into each training example additional information in order to remove ambiguities in the evaluation of the overall response function. Such ambiguities derive from the non-injectivity of the output probabilities, resulting in the presence of multiple parameter points that correspond to the same probability values. In particular, we incorporate into each training example the further set of probabilities P_{ij}^{*} corresponding to the probability values obtained by changing the two voltages of a fixed amount (dV_1, dV_2). Therefore, the single element of the training set is given by $\{\boldsymbol{x}, \boldsymbol{y}\} = \{(P_{ij}, P_{ij}^{*}), (V_1, V_2, V_1 + dV_1, V_2 + dV_2)\}$. The 15% of the data (validation set) is used to compute the actual performances of the trained NN, avoiding overfitting issues, on an independent set of data. The NN performances in reconstructing the device response function can be obtained by studying different figures of merit which quantify the distance between the reconstructed output vector and the real one.

As a follow-up investigation, we studied how the training performances depend on the size of the training set. As a result, we report in Figure 6d the values of the normalized root mean squared error (NRMSE) obtained by training the network with different grid sizes. As expected, increasing the number of data improves the performances on independent test sets.

After such preliminary studies the method has been tested training the NN directly on experimental data. The NN demonstrated optimal results in accurately predicting the experimental data as shown

in Figure 6c. The same NN structure was trained and tested on a different device having the same layout of the previous one. In particular, 80% of the predicted voltages were found to be less than 0.1V from the true values, demonstrating the suitability of the NN for calibrating a series of integrated photonic devices, as in a mass production framework.

Our approach has shown interesting calibration performances with respect to conventional techniques, in terms of both quality of the reconstructed response and required resources. Detailed modeling of the device is not necessary and different devices having the same structure can be efficiently calibrated using the same NN structure. This black-box method is promising for a variety of applications, such as Quantum Metrology. When a voltage-to-phase map is provided it can be optimally adopted for single- and multi-phase estimation problems [Valeri2020].

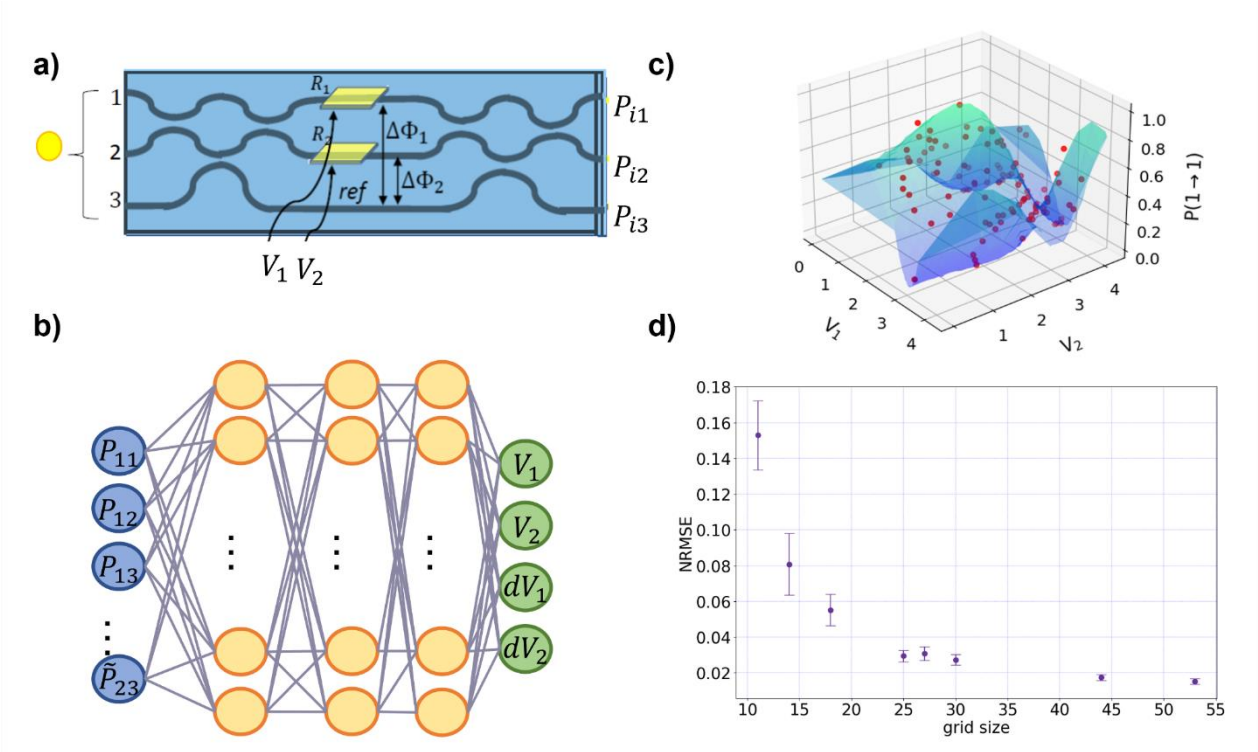

Figure 6. a) Scheme of the integrated circuit: Single photons are injected in one of the 3 input ports of the integrated circuit; at the outputs they are detected by avalanche photodiodes. The output probabilities P_{ij} can be reconstructed as a function of the applied voltages V_1 and V_2 controlling the internal optical phase shift among the interferometer arms. b) Scheme of the NN architecture employed for the calibration process. c) Input-output probability P_{ij} with $i = 1, j = 1$ as a function of the applied voltage pairs. The blue surface represents the experimental measured results while the red dots show the reconstruction performed by the trained NN. d) NRMSE computed over the validation set and achieved with different sizes of the training set.

Programming the reconfigurable 32-mode continuously-coupled interferometer

We applied analogous black-box approaches to the reconfigurable integrated device based on a continuously-coupled waveguide architecture. It comprises 32 optical modes arranged in a 2D triangular lattice and 16 heaters. The main issue to control this kind of reconfigurable circuits regards the difficulty to find an analytical model that links the dissipated powers and the elements of U. Therefore, black-box optimization algorithms or machine learning methods (see Figure 7) could be promising solutions to find a way to control these devices and implement a given transformation.
Our preliminary investigation aimed at finding the function that better approximates the correspondence between a given squared moduli column of the implemented unitary and the set of applied voltages. The RBFOpt algorithm [Costa2018] is a black-box optimization algorithm that exploits the Radial Basis Function method, which builds and iteratively refines a surrogate model of

the unknown objective function. In other words, the algorithm tries to minimize an unknown function $f(\theta)$ (a black-box) that can be evaluate when providing some input values. The θ variables are bounded on a finite interval that is chosen a priori. The utility of RBFOpt is addressed to problems for which each evaluation of the objective function $f(\theta)$ is expensive in terms of computing resources. The task is to find a global minimum of $f(\theta)$ with the minimum evaluation steps. Due to the demanding cost in terms of required resources for evaluating the black-box function and since the function is unknown, there are not first derivatives at disposal, thus RBFOpt works best on problems that are relatively small dimensional and for which the interval for the solution is not too large. In the case of the control over the implemented unitary matrices, we face with an unknown function that links the variations of the squared moduli of the matrix with the variations in the applied voltages. The algorithm performs several evaluations of the black-box function aimed at finding the perfect match to reproduce a target column distribution, chosen by the user. At each evaluation, the algorithm sets the resistors' voltages by choosing the configurations within the pre-given bounds and it collects the output distribution of the squared moduli for the selected column. Subsequently, the algorithm compares the measured output to the target distribution. After some stabilization steps, in which the algorithm tests the operating space, RBFOpt starts to choose the set of applied voltages in order to minimize a quantity that has been chosen a priori. In this particular case, we consider the similarity S between the target distribution and the measured distribution at each step. Thus, the minimization is performed on the quantity 1-S, since we want that the two distributions are as similar as possible (S is close to 1). The measurement for the intensity columns was performed by injecting a single photon in one input of the chip, heralded by the detection of its twin. We tested the performance of the algorithm for two target distribution. The first target is a generic squared moduli distribution for a random Haar matrix. In Deliverable 2.1 and in [Hoch2021], the analysis about the potentiality of the integrated photonic chip in performing random Haar matrices displayed the capability to sample a localized portion of the entire matrix space. Therefore, it is fundamental to take into consideration that the randomly extracted target distribution might be out of range for our optical platform, thus the outcome is not much significant if it is analyzed out of context. After 100 iterations of the algorithm, we obtained that the similarity S is 70%. The second distribution is the one employed as a reference during the first characterization of the chip. Then, the set of applied voltages is known a priori. To check the actual effectiveness, we increased the iterations up to 400. Even in this case, the similarity was equal to 71%, highlighting the limitations of the algorithm. This confirms that the algorithm works not very well with complex response functions [Suprano2021].

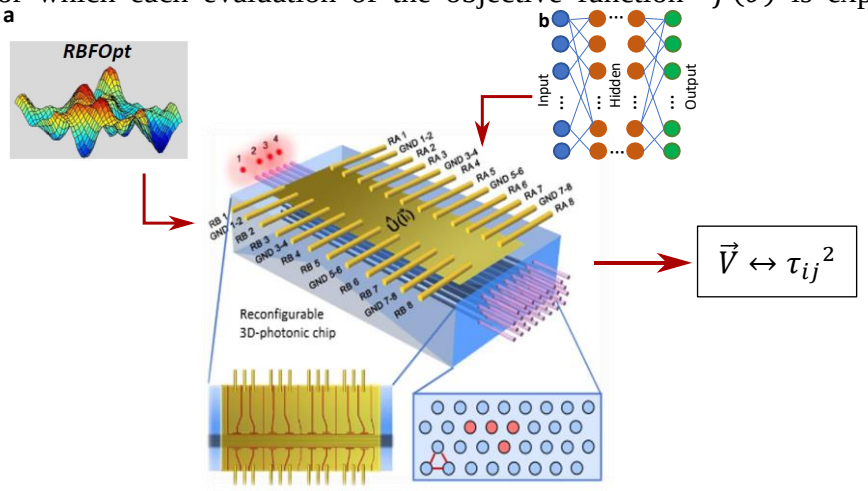

Figure 7 Black-box approaches to control the reconfigurable continuously coupled integrated device. a) The RBFOpt algorithm searches iteratively the configuration of voltages $\vec{V}$ that generates the output distribution most close to the target $\tau_{ij}{}^2$. b) The NN learns from the training data the functions that links the control settings $\vec{V}$ and the squared moduli $\tau_{ij}{}^2$ of the matrix elements.

We then move to a different approach exploiting other machine learning methods. In the previous section dedicated to the calibration of a 3-mode interferometer, we have seen that NN are particularly

feasible to reconstruct an unknown function from labelled data and generalize the learned model for making predictions on new data. In this case, the NN is trained on a dataset composed by labelled measured column distributions. The labels are constituted by the set of applied voltages. The collection of the training set was performed by injecting a single photon in one input of the chip, heralded by the detection of its twin. The input mode was changed among three ports, and this has allowed us to measure a sub-matrix of size 32×3 of squared moduli. The labels, constituted by the applied voltages, are derived from the uniform sampling of the dissipated heats. The dataset is composed of 1535 labelled sub-matrices. We collected the two-fold coincidences between the outputs of the chip and the heralding signal in an integration time of 150 s. The structure of the NN is reported in **Errore. L'origine riferimento non è stata trovata.**.

Layer	Input and Output dimension
Input linear layer (activation function: $tanh$)	(96, 1024)
2nd linear layer (activation function: $tanh$)	(1024, 2048)
3rd linear layer (activation function: $SeLU$)	(2048, 248)
Output linear layer (activation function: $ReLU$)	(248, 16)

Table 1. In the table, the structure of the NN architecture that was employed for the control of the squared moduli sub-matrix. The input is a vector of dimension $96 = 32 \times 3$ corresponding to the measured single-photon distributions in the experiment. The output is a vector with 16 components that contains the voltages to be applied to obtain the given sub-matrix.

During the training stages, we obtained an average similarity S of 95.8% between predicted voltages and test dataset labels, with maximum value of S at 99.9% and minimum value of 87.7%. These results show the ability by the NN to generalize the platform model. In addition, we tested the trained NN over the reference distribution of intensity from one input, employed during the first alignment and calibration of the chip. We set the power supply that controls the electrical circuit of the heaters with the voltages predicted from the NN for this distribution. Then, we measured the intensity again and we obtained a similarity of 96.6% with the reference distribution. A qualitative comparison is inserted in Figure 8.

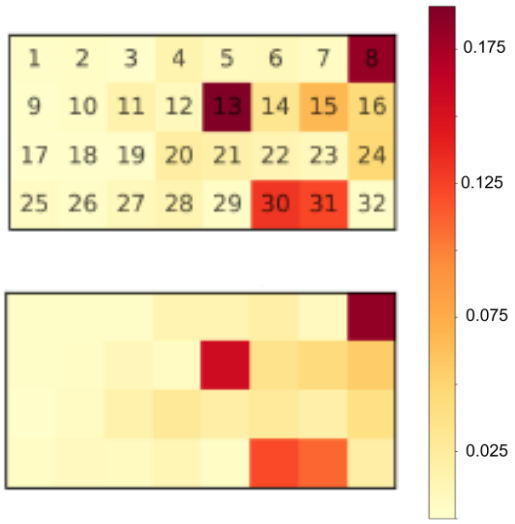

Figure 8. In the two color-maps a single-input intensity distribution in the 32 output modes. Above the reference distribution, below the distribution measured with the voltages predicted from the network.

Complete toolbox: conclusions

The promising outcome of the NN in the squared moduli-voltages prediction opens the pathway to the full control of the photonic chip. Indeed, the previous measurements were performed by sending single-photon input, thus enabling for the NN the reconstruction of the map between voltages and unitary matrix moduli. By adding further measurements to the process, it is possible to extend the calibration procedure to acquire information also on the map between voltages the complex phases of the transformation. In this perspective, it is necessary to find an optimal strategy that allows us for the collection of the phase dataset for different voltages configurations. More specifically, for the 32-mode device the dataset should be composed of two 32×3 matrices, one containing the squared moduli and one containing the phases, both labelled to be linked with the corresponding set of applied voltages. The question that arises at this point is how to measure the complex phases of the unitary matrices and thus prepare the training dataset. As previously discussed, measurements of the HOM visibilities requires long measurement runs for each sub-matrix, leading to large acquisition times for the training set. An alternative solution

which can be more effective in larger devices is the previously introduced measurement of the cross correlations with classical light proposed in the previous section. The time needed for their estimation is remarkably shorter. Therefore, future steps will be the arrangement of the cross-correlation measurement setup in Figure 4 for the 32-mode integrated interferometer.
From our analysis emerges that learning methods are the most effective for the control and the calibration of large-scale integrated devices. Other algorithms such as the random forest regressor or genetic algorithms can be investigated for the task. Regarding genetic algorithm [Spagnolo2017], they have been shown to be applicable as a minimization toolbox for static circuits. However, they rely on some a-priori modeling of the device response function, which is not trivial for a dynamical scenario. As a general note, other machine learning schemes that do not involve neural networks are less expensive in terms of computational cost and easier to interpret. On the other, they can fail when the space of the parameters is too large. Other routines for dimensionality reduction to be applied first to the data, such as principal component and linear discriminant analysis, could mitigate such a limitation. Notwithstanding, in large scale optical circuits, the NN approach remains the most suitable and effective for this task.

References

[Polino2019] E. Polino, et al., Optica **6**, 2334-2536 (2019).
[Cimini2021] V. Cimini, et al., Phys. Rev. App. **15**, 044003 (2021).
[Valeri2020] M. Valeri, et al., npj Quantum Inf. **6**, 92 (2020).
[Laing2012] A. Laing et al., arXiv:1208.2868 (2012)
[Tillmann2016] M. Tillmann, et al., Journal of Optics **18**, 114002 (2016).
[Spagnolo2017] N. Spagnolo, et al., Scientific Reports **7**, 14316 (2017).
[Sinkhorn1967] R. Sinkhorn et al., Pacific Journal of Mathematics **21**, 343–348 (1967).
[Idel2016] M. Idel, arXiv:1609.06349 (2016)
[Hong1987] C.-K. Hong, et al., Phys. Rev. Lett. **59**, 2044 (1987)
[Hoch2021] F. Hoch et al., arXiv:2106.08260 (2021)
[Costa2018] A. Costa et al., Math. Programming Comput. **10**, 597–629 (2018).